

The Leading Edge, v. 22, n. 3, pp. 232-237, 2003

Imaging Crust and Upper Mantle Seismic Structure in the Southwestern United States Using Teleseismic Receiver Functions

David Wilson¹, Richard Aster¹, and the RISTRA Team

¹Department of Earth and Environmental Science and Geophysical Research Center, New Mexico Institute of Mining and Technology, Socorro, NM

Introduction. The Rio Grande Rift Seismic TRAnsect (RISTRA) (Figure 1) is designed to image and interpret crust and mantle structures beneath the SW U.S., including the nature of the Colorado Plateau and Rio Grande rift. Key questions include the nature of crustal and mantle structures and thermal conditions beneath one of the more dramatic continental rifts on Earth, and clues to understanding the anomalously unextended Colorado Plateau, which is currently surrounded by the predominantly extensional deformation of the American west.

The data collecting stage of RISTRA provided an exceptional 18 months (1999-2001) of broadband (Streckheisen STS-2 120 s seismometers) teleseismic IRIS PASSCAL data along a 950-km great-circle transect of 54 sites with 18 ± 3.6 km station spacing with endpoints near Lake Powell, UT and Pecos, TX. The northwest-southeast trending transect was oriented parallel to the azimuth of the very active western Pacific seismogenic zones. Analysis applied to this seismic data set includes surface wave dispersion inversion for crustal and mantle structure, teleseismic body wave tomography, and teleseismic mantle anisotropy. Here we discuss the use of RISTRA data to examine lithospheric structure using *P*-to-*S* mantle and crustal forward scattering, observed in the *S* phases immediately following (several tens of seconds) the teleseismic *P* arrival (Figure 2). We migrate these signals to produce *P*-to-*S* converted mode images of the structure along the RISTRA array.

RISTRA geologic history spans nearly 2 b.y. The crustal basement of the region was assembled in a series of continental accretionary events in which island arcs, oceanic plateaus, and marginal basin terranes were adhered to the continent from approximately northwest to southeast (Bowring and Karlstrom, *Geology*, 1990). RISTRA thus follows the approximate continental age accretionary gradient to cross two major Proterozoic province boundaries, the Mazatzal and Yavapai (1.6-1.7 b.y. old and 1.7-1.8 b.y. old, respectively) suture in the northwest, and entering the Grenville (≈ 1.1 b.y. old) province near the eastern edge of the Delaware basin in the southeast.

The RISTRA region underwent east-west compression during the Mesozoic (80-50 m.y.a.) Laramide orogeny as the Farallon slab was subducting beneath western North

America. During this period the slab is thought to have been subducting at a low angle (e.g., Dickinson and Snyder, GSA memoir, 1978). Between approximately 43 to 30 m.y.a., as the initiation of the San Andreas fault was shutting off subduction, a portion of the slab may have detached, spurring the dramatically enhanced volcanism in the southwestern U.S. referred to as the "ignimbrite flare-up" (Humphreys, Geology, 1995). During the past 30 m.y. the region has been in extension, along with much of interior western North America. This regional extension stimulated the formation of the Rio Grande rift along a concentrated north-south zone of extension, while leaving the adjacent Colorado Plateau relatively undeformed. Rifting is thought to have formed in at least two stages (e.g., Olsen et al., Tectonophysics, 1987). An initial stage at 30 to 20 m.y.a., associated with low angle faulting and doming in the crust, may have been caused by upper-mantle asthenospheric upwelling and thermal erosion of the lithosphere. After perhaps 10 m.y. of quiescence, a second stage of rift activity resumed with high-angle normal faulting and alkalic basaltic volcanism. During the past 4 m.y., there has been increased volcanism along the Jemez Lineament, which approximately follows the Yavapai/Matzatzal suture.

Receiver Functions. As earthquake body waves travel through the Earth, they produce a sequence of reflections, refractions, and conversions (e.g., from P to S waves) at discontinuities and/or rapid transition zones separating regions of differing seismic impedance. Receiver function seismogram processing emphasizes *P*-to-*S* converted phases from such interfaces while removing source complexity through the deconvolution of horizontal component seismograms by corresponding vertical component seismograms. The primary assumption of the receiver function methodology is that the initial seismic excitation of upper mantle and crustal structure is nearly a plane *P* wave; this is a reasonable assumption for a teleseismic wavefront following passage through a relatively homogeneous mid-mantle (See Pavlis' article in this issue for a more detailed discussion of seismic processing and imaging of receiver functions).

For a typical RISTRA receiver function, four dominant converted/refracted modes of ray propagation are commonly observed (Figure 3): 1) Direct *P*, observed as a prominent pulse near zero time. 2) Direct, *P*-to-*S* (*Ps*) generated at each discontinuity; 3) The *PpPs* mode resulting from incoming *P* refracting as *P* at a discontinuity, reflecting downward as *P* off the earth's free surface, then converting/reflecting upwards as *S* at each discontinuity; 4) The (simultaneously arriving) *PpSs* and *PsPs* modes resulting from incoming *P*, refracting/converting as *P* or *S* at a discontinuity, reflecting downward as *P* or *S*, off the earth's free surface, and finally reflecting upwards as *S* at each discontinuity. All of the above reflected/converted modes exhibit distinct moveout as a function of source-receiver offset. By measuring these moveouts (assuming a locally flat layered structure), it is possible to estimate local depth and average V_P/V_S ratio between the surface and the discontinuity associated with each mode. In practice, individual modes can be difficult to observe and identify on individual traces, so stacking of many events from a variety of azimuths and ranges is employed, and a search performed (e.g., by first fixing an initial *P*-wave velocity structure) over a range of depths to the discontinuity and V_P/V_S ratios (Zhu and Kanamori, JGR, 2000). Parameters where arriving energy stacks most constructively provide best estimates of discontinuity depth and V_P/V_S ratio, and the estimates of the standard deviation for such determinations

can be calculated from the width of stack maxima.

Figure 4 shows estimated depths and V_P/V_S ratios determined from moveout analysis. These results were obtained using a starting P -wave velocity model constructed from prior refraction surveys and surface wave experiments in the region, as well as extensive well log data and sediment thickness maps from the Delaware and San Juan basins. Exploration industry measurements were especially valuable in the accurate characterization of these deep basins. Crustal thickness is found to range from 45 to 50 km beneath the Colorado Plateau (stations NM34-UT54), thinning to a minimum of approximately 35 km near the center of the Rio Grande rift (NM22-NM30). The centering of the shallowest crust on the rift axis argues for pure shear thinning of the crust during Cenozoic rifting, as opposed to simple shear controlled by master detachments. Crustal thickness beneath the Great Plains (TX01-NM20) shows variability over shorter distances, ranging from 43 to 50 km. The overall average crustal V_P/V_S ratio beneath RISTRA is 1.78 (Poisson's ratio (σ) of .27), with the highest ratios (up to $V_P/V_S=1.84$; $\sigma=.29$) estimated between stations NM16-NM22. High crustal V_P/V_S ratios may indicate an overall more mafic crustal composition, and NM16-NM22 are located directly adjacent to the major Tertiary igneous intrusions of Sierra Blanca and the Capitan Mountains. High V_P/V_S ratios ($V_P/V_S=1.8$; $\sigma=.28$) are also observed for stations TX01-NM08; however these stations are located on the thick sediments of the Delaware basin which significantly raises overall crustal V_P/V_S average.

Receiver Function Imaging. Receiver functions were first applied in the late 1970's at solitary stations to obtain local, 1-dimensional structural estimates (e.g., Langston, JGR, 1979). Since then, the number of stations in temporary seismic experiments has increased substantially due to growth in availability of portable broadband instruments through IRIS PASSCAL and other resources. It is now possible to generate increasingly detailed 2- and 3-dimensional images of fundamental structures, such as the Moho and upper mantle transition zone discontinuities near 410 km and 670 km depth. A first-order method of generating receiver function 2-dimensional cross sections is to use the transmission analog of the common conversion point (CCP) stacking used in exploration seismology. A receiver function CCP image is created by back-projecting the recorded signal along the theoretical ray path and stacking the amplitude information into lateral and vertical bins. A cross section is then generated by taking the mean sample value (or some other central tendency measure) in each bin. Although CCP imaging transforms the data into offset and depth space, it does not correct for diffracted energy. Thus, if significant lateral structural heterogeneity is present the resulting image may poorly represent true lateral earth structure.

RISTRA produced multicomponent broadband seismic data along a transect that is one of the longest (950 km) and most densely occupied (approximately 18 km interstation spacing) of any such PASSCAL experiment to date. It is thus well suited for developing and applying more realistic seismic migration techniques to teleseismic receiver function imaging. In regions of highly heterogeneous lateral Earth structure, migration methodologies are designed to properly move seismic trace energy (e.g., P -to- S conversion amplitudes in receiver functions) to their true subsurface positions in time or depth, and to correspondingly suppress artifacts generated by diffracted energy that will be incorrectly imaged in CCP and other simpler stacking techniques.

Here, we migrate each of the Ps , $PpPs$, and $PpSs + PsPs$ modes using a Kirchhoff style migration, thus characterizing the output model as a grid of point scatterers. Travel times for the direct converted mode (Ps) are calculated by assuming a plane P wave incident from below the model that converts to shear wave energy at every possible scattering point. Travel times for multiples are similarly calculated by modeling their appropriate ray path geometries. Basins, especially, trap seismic energy and thus produce strong multiples that can contaminate the images. To suppress such multiples, the three migrated modes are migrated onto three separate output grids which can then be stacked to suppress multiples arising from any single mode. We restrict the migration aperture (incident angle of propagating seismic energy) and frequency content of the data to be consistent with the seismic wave equation and to prevent aliasing of the imaged data. For imaging at crustal levels (to 60 km depth) the direct converted mode (Ps) has maximum energy at approximately 1-2 Hz, while the crustal multiples have the most energy at 0.25-0.5 Hz. Ps energy from deeper mantle discontinuities at 410 km and 670 km depth has greatest amplitude at periods of 4 to 6 s.

Figure 5 shows migrated teleseismic receiver functions for RISTRA using the velocity model calculated from phase moveout analysis. The top panel shows the migrated direct (Ps) phase, the middle panel is a stack of Ps and $PpPs$ images, and the bottom panel is a stack of Ps , $PpPs$, and $PpSs + PsPs$ images. Stacks are performed using 4th root nonlinear stacking, so that large amplitudes in the image will only occur when the Ps , $PpPs$, and the (negative of the) $PpSs + PsPs$ migration images have the same polarity. In the top panel, strong reverberations from the Delaware basin are evident and interfere with Moho and deeper direct conversion structural information. However, as the other migrated images are stacked in, these reverberations become greatly attenuated, while direct converted energy mapped to its correct depth is enhanced (e.g., the basement contact at approximately 6 km depth in the center of the Delaware basin). The composite migrated image of the Moho shows dramatic thinning of approximately 10 km under the central rift, as well as intriguing second-order features that suggest significant short-wavelength Moho topographic and impedance contrast variability (e.g., thickness changes of up to 7 km over lateral distances of less than 100 km). The direct converted Moho phase beneath the Rio Grande rift suggests a single discontinuity. However, beneath the Colorado Plateau and Great Plains the phase is more complex, perhaps indicative of lower crustal layering and/or gradational Moho.

A migrated receiver function image of the upper mantle (Figure 6) shows negligible topography on the 410 km (exothermic, α -olivine to β -spinel) and 670 km depth (endothermic; γ -spinel to perovskite) mantle transition zone discontinuities, which indicates a lack of a localized thermal anomaly under the region at these depths. A strong increase in temperature associated with a deep mantle upwelling would be expected to compress the transition zone thickness by around 15 km per 100° C. This suggests that the thermal signature of the Rio Grande rift may be predominantly confined to the uppermost mantle.

Conclusions. RISTRA is providing images of unprecedented resolution of crustal and mantle features associated with the tectonic history of the Rio Grande rift and Colorado Plateau regions to depths extending through the upper mantle. Some key discoveries have included the most detailed examination of Moho and upper mantle dis-

continuities in this region, evidence for near pure shear crustal thinning during Cenozoic rifting, and apparent confinement of hot upper mantle to above 400 km depth.

Implications for future passive seismic array deployments. Well-developed exploration data processing techniques, such as prestack Kirchhoff seismic migration, can be applied successfully to converted phase, transmission geometry, passive source seismic experiments on a regional scale, while a suite of migrated images corresponding to different phases can be stacked to reduce multiple-generated artifacts. One clear direction as instrumental resources continue to expand is to exploit 3-dimensional imaging using these methodologies. Another ongoing development (currently being pursued for RISTRA) is to jointly utilize velocity modeling results from teleseismic *P*- and *S*-wave tomography, coupled with surface wave phase and/or group velocity constraints to further improve migrated image accuracy.

Suggested Reading.

The isolation of receiver effects from teleseismic *P*-wave-forms, by C. Ammon, (Bull. Seism. Soc. Am., 1991).

The Rio Grande Rift, by Baldrige et al., from Continental Rifts: Evolution, Structure, and Tectonics, Olsen, K.H., ed., (Developments in Geotectonics 25, Elsevier, 1995).

Acknowledgements. The RISTRA Team is Rick Aster (New Mexico Tech), W. Scott Baldrige (Los Alamos National Laboratory), Wei Gao (University of Texas, Austin), Rengin Gok (Lawrence Livermore National Laboratory), Steve Grand (University of Texas, Austin), Jim Ni (New Mexico State University), Eric Sandvol (University of Missouri, Columbia), Steve Semken (Dine College), Mike West (New Mexico State University), and Dave Wilson (New Mexico Tech). We thank the PASSCAL Instrument Center at New Mexico Tech for planning and data processing assistance. We also thank the dozens of private landowners, the New Mexico State Land Office, the United States Forest Service, the United States Bureau of Land Management, the United States Fish and Wildlife Service, the Southern Utah Wilderness Alliance, Isleta Pueblo, Laguna Pueblo, and the Navajo Nation for assistance in the permitting and siting of these instruments. Persons wishing to conduct geological investigations on the Navajo Nation must first apply for and receive a permit from the Navajo Nation Minerals Department, PO Box 1910, Window Rock, Arizona, 86515, 928-871-6587. This study was supported by NSF grants EAR 9707190 and EAR 9706094. We also thank Los Alamos National Laboratory IGPP and the NMSU Arts and Sciences Research Center for their support. Essential RISTRA field assistance was provided by Joe Leon, Eric Matzel, Richard Rapine, Frederik Tilmann, Wei-Chuang Huang, Al Blackhorse, Laurecita Luna, and Dueker's Diggers.

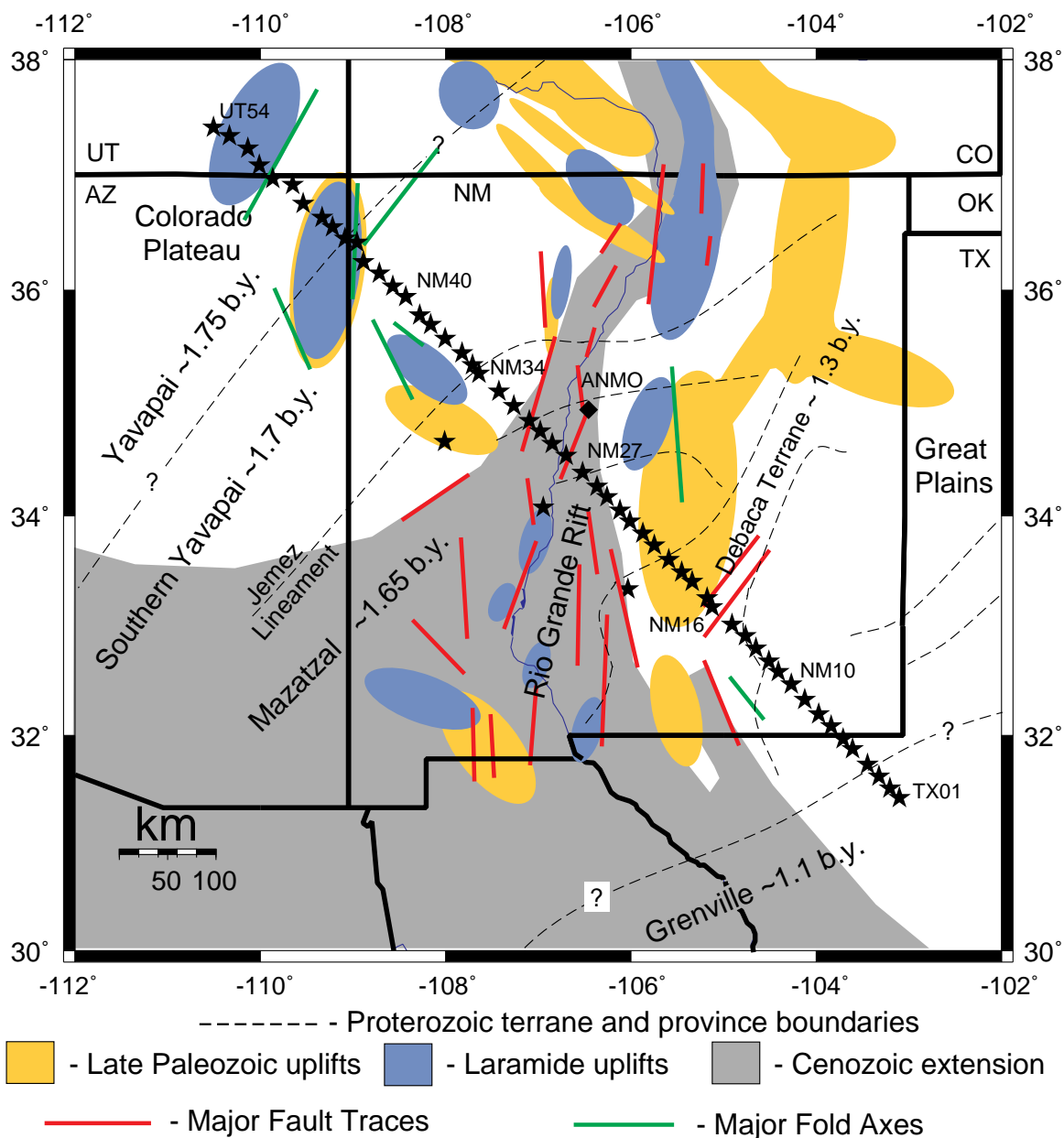


Figure 1: Regional tectonic map with RISTRA station locations. Stars show the 54 main transect station locations and the diamond shows the location of the Global Seismic Network borehole station ANMO. Stations TX01-TX06 lie in Texas, NM07-NM44 in New Mexico, AZ45-AZ50 in Arizona, and UT51-UT54 in Utah.

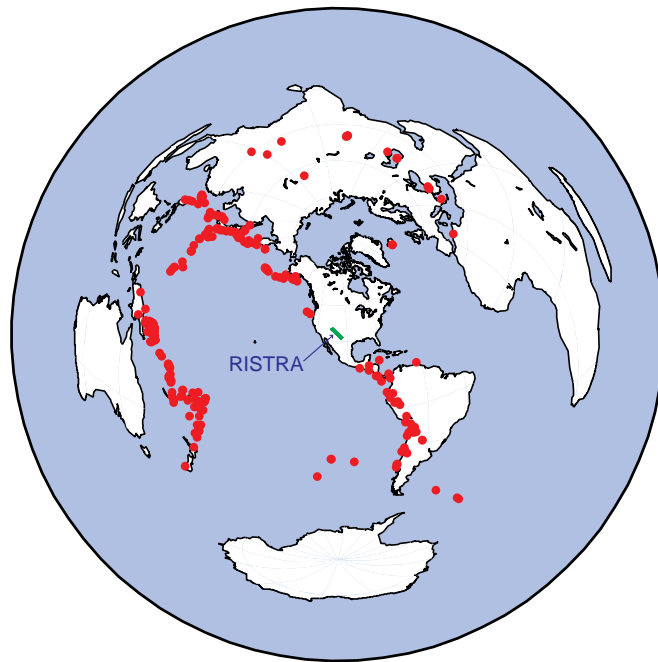


Figure 2: Global distribution of the 285 earthquakes (red points) with $m_b \geq 5.6$, recorded during the RISTRA network deployment, which have suitable offsets for calculating the 8361 receiver functions used in this study. We use teleseisms from epicentral distances of $25^\circ - 105^\circ$, which have incident angles ranging from approximately 40° to 15° at the base of the crust. The RISTRA seismometer deployment is shown in green as great-circle swath.

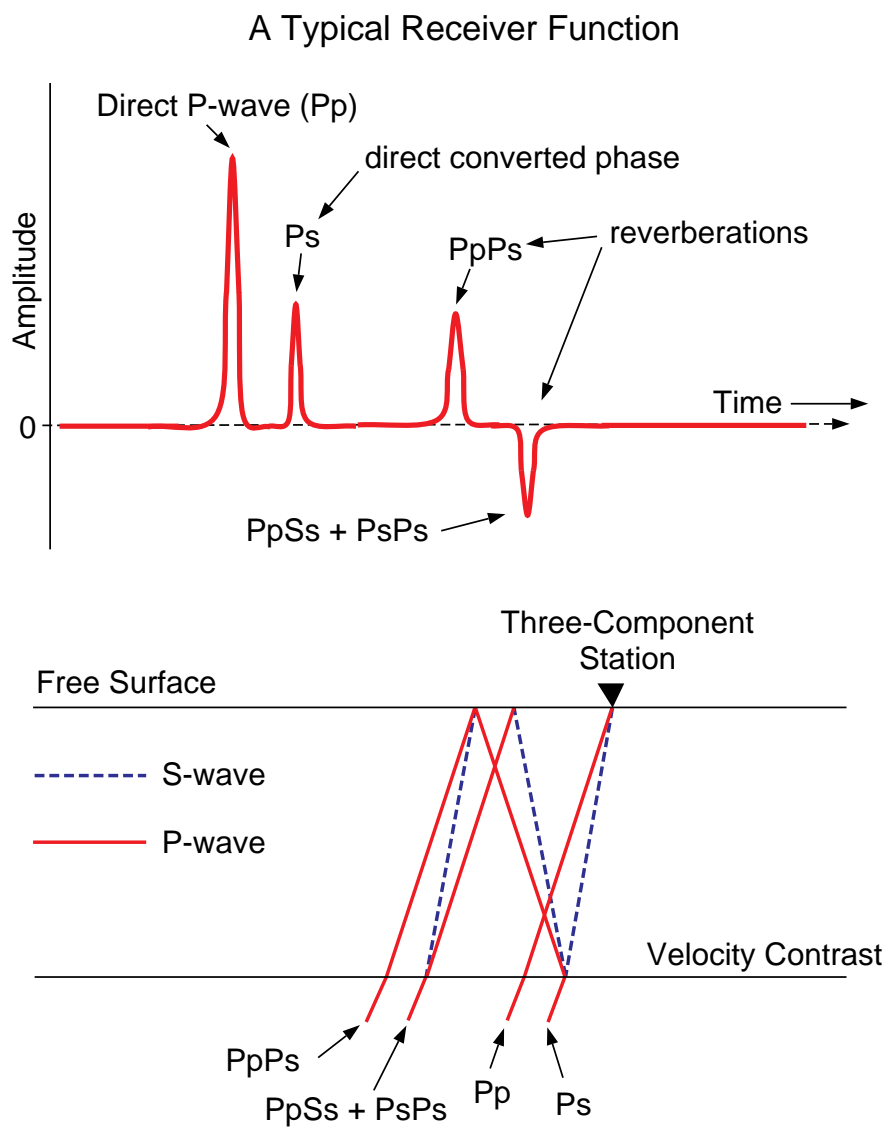


Figure 3: Raypaths for direct/converted propagation modes typically seen in RISTRA receiver functions.

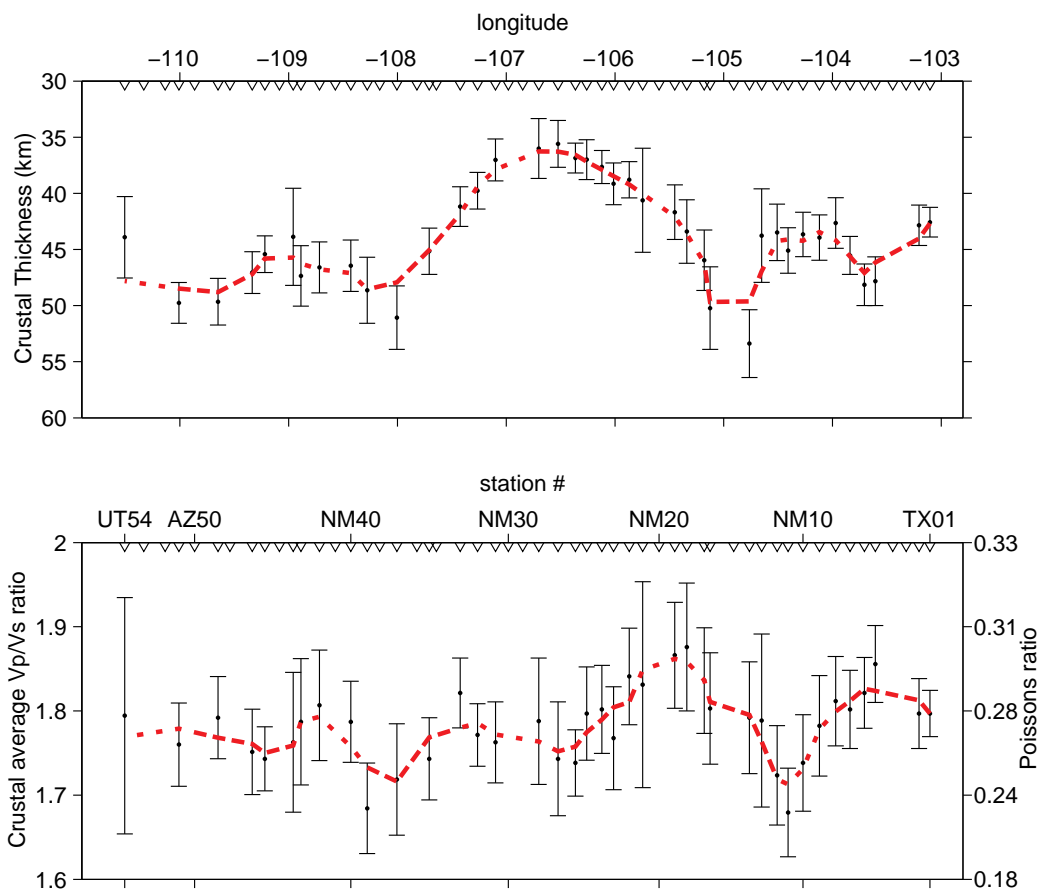


Figure 4: Crustal thickness and average V_P/V_S ratios determined from moveout analysis of primary and reverberated P -to- S converted modes. The red dashed line shows a 3-point weighted mean.

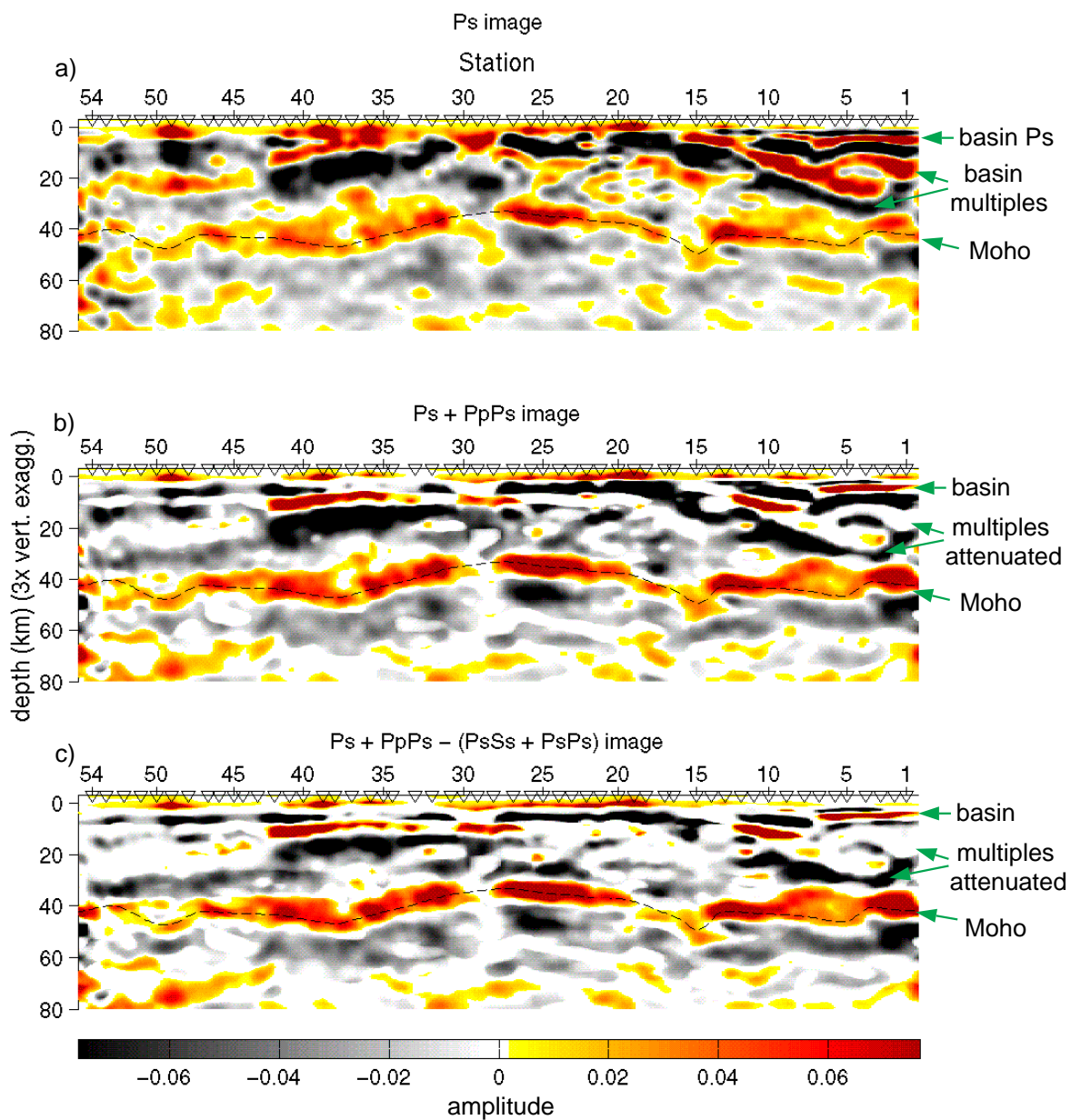


Figure 5: Migrated crustal cross sections. Reverberations from the sedimentary basins along the network interfere with deeper structural information (a). As more migrated phases are stacked in (b and c) the reverberations become greatly attenuated while energy mapped to its correct depth is enhanced. The dashed line is the base of the crust in the velocity model.

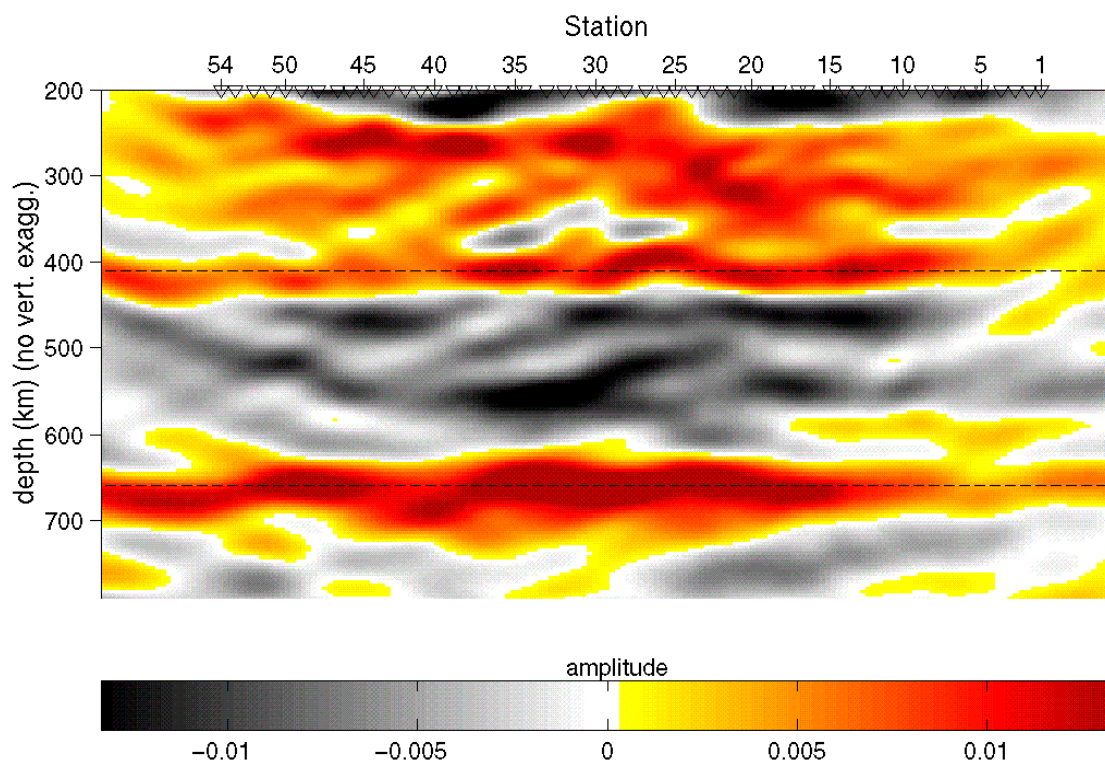


Figure 6: Migrated upper mantle cross section showing negligible topography on the 410 and 670 km depth mantle transition zone discontinuities, which indicates a lack of a localized thermal anomaly under the region at these depths. Dashed lines are at 410 and 670 km for reference.